Active EMI Suppression with Adapted Cancellation Signals for a Buck Converter in Varying Modes of Operation

Tobias Dörlemann[1], Andreas Bendicks[1], Stephan Frei[1]

[1] On-board Systems Lab, TU Dortmund University, Germany

Corresponding author: Tobias Dörlemann, tobias.doerlemann@tu-dortmund.de

Abstract

Many modern power electronic systems make use of fast switching semiconductors for energy conversion and distribution. Steep switching slopes for high efficiencies may cause high levels of electromagnetic emissions. Conducted emissions are conventionally reduced by applying heavy and bulky passive filter components. The basic concept of active filtering aims at a destructive interference between the emissions (noise) and a generated anti-noise signal and is one idea to overcome the disadvantages of passive filter components. In this contribution, a self-adapting, FPGA-based active EMI cancellation system using artificially synthesized cancellation signals is investigated for the first time during a buck converter's transient changes in operation.

1 Introduction

Fast-switching power electronic converters can be significant sources of **e**lectro**m**agnetic **i**nterferences (EMI). To reduce the EMI and to comply with international standards in **e**lectro**m**agnetic **c**ompatibility (EMC), e.g. CISPR 25 for vehicles [1], passive filter components are conventionally applied [2]. Because these passive filter components usually suffer from their high weight and volume, active EMI filtering concepts (e.g. [3] – [5]) have been elaborated that aim for a destructive interference between noise and anti-noise signals.

To yield a stable destructive interference, the anti-noise signal must equal the noise signal with opposite sign. Therefore, in feedforward and feedback active filtering concepts, noise signals are measured, inverted, amplified and back-injected as anti-noise signals. Due to time constants and unavoidable signal propagation delays, the perfect fit between noise and anti-noise signals is limited. Accordingly, the achievable noise suppression is also limited [6].

By injecting artificially synthesized and synchronized anti-noise signals, the limiting influence of time constants and signal propagation delays can be compensated. Time constants can be compensated by shaping the anti-noise signals. Signal propagation delays can be compensated by injecting the anti-noise signals before the noise occurs. For a stable destructive interference, noise and anti-noise signals must be synchronized by appropriate means. Since the fit between these signals is significantly improved by this measure, high EMI reductions can be achieved in a wide frequency range [6].

One approach to realize an active cancellation system with synthesized and synchronized signals is to use methods in frequency domain. In e.g. [7], the anti-noise signal is calculated by measuring and identifying the noise signal with the help of an off-line **f**ast **f**ourier **t**ransform (FFT) and taking the transmission path's influence on the injected anti-noise signal into account. Because of the needed calculation time, this method requires periodic noise signals and a perfect synchronization between noise and anti-noise signal source. This system is well suited to show the potential of using synchronized and synthesized cancellation signals, but it is limited by its requirement of periodic noise signals.

Another approach are single-frequency adaptive notch filters that have originally been designed for active noise cancellation approaches in the acoustic domain (e.g. [8] – [9], [15]). Here, the anti-noise signal is artificially synthesized from sine waves that shall suppress the corresponding harmonic of the noise signal (e.g. [10] - [12]). By adaptively adjusting the amplitudes and phases of each sine wave, the influence of time constants and signal propagation delays can be

compensated. This adjustment can be done by appropriate optimizers that observe the residual noise (superposition of noise and anti-noise). Multiple harmonics of the noise can be compensated by applying a set of notch filters in parallel and superposing all anti-noise sine waves.

In, e.g., [10] - [12], the single-frequency adaptive notch filter is applied to a buck converter with constant load and supply conditions, constant duty cycle and constant switching frequency. In [13] and [14], it is applied to a **p**ower **f**actor **c**orrection (PFC). In this application, the duty cycle varies with the mains' voltage, but all other conditions are still constant. These investigations show the performance of the method during stationary modes of operation, but practical systems are also exposed to transient changes. Since the EMC must also be fulfilled during such dynamic modes of operation, they are investigated in this work. A buck converter will be used as an exemplary demonstrator. The following abrupt changes will be investigated:

- Turn-on of the active cancellation system,
- Change of the buck converter's duty cycle,
- Change of the buck converter's load.

At first, the fundamental theory of single-frequency adaptive notch filters is explained in Section 2, while the FPGA-based realization of the active EMI cancellation system and the test setup are described in Section 3 and Section 4, respectively. In Section 5, the dynamic behavior of the adaptive notch filter implementation is investigated with help of time-domain measurements and spectrograms. In Section 6, the limits and potentials of the method are investigated with the help of EMI receiver measurements. Finally, a conclusion and an outlook are given in Section 7.

2 Theory of single-frequency adaptive notch filters

Adaptive notch filters can be classified as narrowband feedforward **a**ctive **n**oise **c**ontrol (ANC) systems and have been extensively examined in acoustics, e.g. [8] and [9].

The concept of adaptive notch filters bases on the digital synthesis of a sinusoidal signal (cancelling sine wave) for every noise signal frequency to be mitigated. At every instant of time, all cancelling sine waves in parallel are adapted in amplitude and phase, superimposed, digital-to-analog-converted and injected as an anti-noise signal. This anti-noise signal is intended to destructively interfere with the corresponding noise signal frequency components.

In Fig. 1, an ideal time-discrete single-frequency adaptive notch filter algorithm is depicted. An orthogonal system is created by synthesizing an arbitrary time-discrete cosine signal $x_0(n)$ and an arbitrary time-discrete sine signal $x_1(n)$ with frequency f_0 in parallel. Both reference signals $x_0(n)$ and $x_1(n)$ are multiplied by a weighting factor $w_0(n)$ or $w_1(n)$, respectively. Subsequently, the resulting products are superimposed and inverted to form the anti-noise signal $y(n)$. By adapting the filter weights in every single time step as shown in (1) and (2), the resulting anti-noise signal $y(n)$ can be adjusted in amplitude and phase. This adaptation is achieved with help of the **L**east **M**ean **S**quare (LMS) algorithm that bases on the concept of gradient descent.

$$w_0(n+1) = w_0(n) + \mu \cdot e(n) \cdot x_0(n) \qquad (1)$$

$$w_1(n+1) = w_1(n) + \mu \cdot e(n) \cdot x_1(n) \qquad (2)$$

In [8, 9], the $1/e$ time constant τ of the adaptation process is approximated under ideal assumptions and is given in (3). Here, T_s represents the sample time of the time-discrete system, while A represents the amplitude of both reference signals $x_0(n)$ and $x_1(n)$ (in this work: $A = 1$). The step size parameter μ determines the adaptation speed of the algorithm. While a smaller step size μ results in more precise results, a larger step size enables a faster adaptation.

$$\tau \leq \frac{2T_s}{\mu A^2} \qquad (3)$$

Hence, regarding dynamic noise signals, a bigger step size μ is beneficial to follow the changes. Nevertheless, if the step size μ is chosen too large, the anti-noise signal's precision can be noticeably reduced, or the adaptive notch filter can even become unstable. A stability analysis of ideal adaptive notch filters can be found in, e.g., [9].

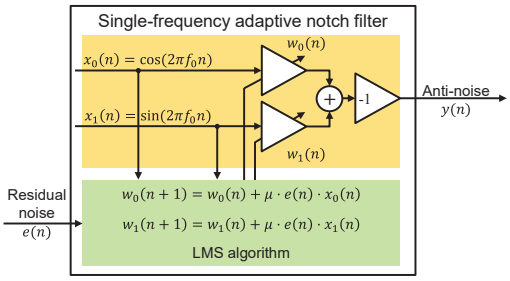

Fig. 1: Single-frequency adaptive notch filter with LMS algorithm.

In practical applications, the noise and anti-noise signals are not directly superimposed. The anti-noise signal must first be digital-to-analog converted and injected. Then, it propagates through the overall system and superposes itself with the noise. The resulting residual noise must be sensed and analog-to-digital converted. So, the complex transfer function for the anti-noise signal path contains time constants and delay times. This transfer function influences the adaptive notch filter's behavior in real applications and has to be considered in the design of the algorithm. Especially the resulting delay time for each cancelling sine wave (that also comprises phase shifts) is critical for the stability of the algorithm.

To avoid instabilities due to this delay time, the adaptive notch filter's LMS algorithm is implemented as a delayed LMS (DLMS) algorithm ([9] and [16]) as shown in (4) and (5). In this adaptation process, Δ is an estimation of the corresponding delay time.

$$w_0(n+1) = w_0(n) + \mu \cdot e(n) \cdot x_0(n-\Delta) \quad (4)$$

$$w_1(n+1) = w_1(n) + \mu \cdot e(n) \cdot x_1(n-\Delta) \quad (5)$$

To ensure the stability of the adaptive notch filter, the error between the estimation Δ and the actual delay time must be smaller than $\pm 90°$ [8, 9]. In case of an estimation error smaller than $\pm 40°$, the convergence speed of the algorithm is theoretically only slightly affected [9, 17].

Regarding the convergence speed of the algorithm, the time delay between anti-noise signal synthesis and residual noise signal measurement should be as short as possible to reduce the notch filter's dead time.

3 FPGA-based realization of the active EMI cancellation system

In this work, an FPGA development board Red Pitaya STEMlab 125-14 is used as a hardware basis for the active EMI cancellation system. This development board provides fast analog-to-digital and digital-to-analog converters with a sample rate of 125 MS/s and a vertical resolution of 14 bit in combination with a **F**ield-**P**rogrammable **G**ate **A**rray (FPGA). The used FPGA-based implementation comprises six single-frequency adaptive notch filters with DLMS-adaptation algorithm in parallel, as illustrated in Fig. 2. In this work, all six adaptive notch filters are parametrized with the same step size μ.

With help of a sensing circuit, the residual noise signal is measured between the EMI source and the EMI sink. The measured residual noise signal is analog-to-digital-converted and passed to the FPGA-implementation of the six parallel adaptive notch filters. Each adaptive notch filter synthesizes an anti-noise orthogonal system and optimizes its weighting factors to minimize the residual noise regarding its considered anti-noise frequency. The anti-noise frequencies of all six adaptive notch filters in parallel are superimposed inside the FPGA logic to form the anti-noise signal. This anti-noise signal is passed through the digital-to-analog-converter and injected into the system.

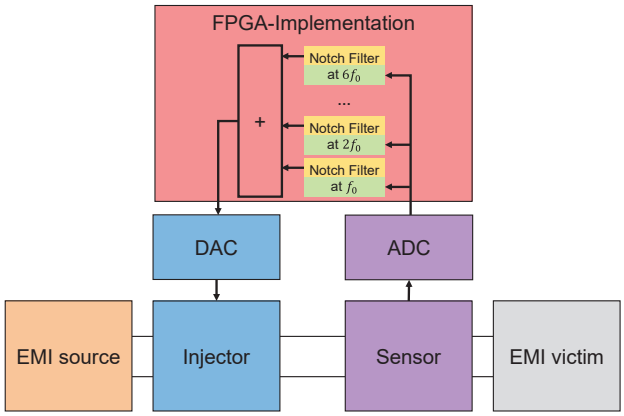

Fig. 2: Topology of the FPGA-based active EMI cancellation concept.

4 Test setup: DC/DC buck converter

The following investigations make use of a test setup consisting of a 48 V / 12 V buck converter powered by a 48 V voltage source and driving an ohmic load. The schematic can be found in Fig. 3. Photographs of the of the overall test setup and the inside of the **D**evice **U**nder **T**est's (DUT) box can be found in Fig. 4 and Fig. 5.

An arbitrary function generator is used to generate the buck converter's trapezoidal control signal with a fundamental frequency of $f_0 = 300\,\mathrm{kHz}$. To enable a standardized measurement of the resulting noise voltage, an artificial network is placed between the 48 V voltage source and the buck converter (according to CISPR 25, [1]). For evaluation purposes, the resulting noise signal is measured by an oscilloscope with 50 Ω-termination or an EMI receiver (that intrinsically has a termination of 50 Ω) at the artificial network's measurement port.

The FPGA-based adaptive notch filter implementation is realized as described in

Section 3. For each of the control signal's first six harmonics $(f_0 = 300\,\mathrm{kHz}, \ldots, 6f_0 = 1.8\,\mathrm{MHz})$, one of the six parallel adaptive notch filters synthesizes a cancelling sine wave. For adaptation purposes, the residual noise signal is measured, while the nominal voltage of 48 V is blocked by a capacitor. To prevent an overdrive of the ADC due to high-frequency components (that are not actively cancelled out), a low-pass filter is applied. To dampen resonances, a 3 dB attenuator is added. The generated anti-noise signal is digital-to-analog-converted and injected into the test setup using an inductive coupler. A possible DC-offset of the anti-noise signal is blocked by a capacitor. Further details regarding the used sensing and injecting circuits can be found in [12].

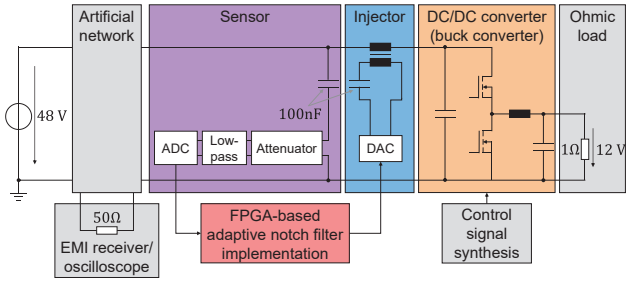

Fig. 3: Schematics of the test setup.

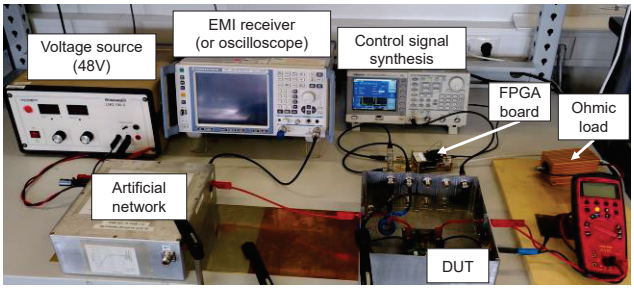

Fig. 4: Photograph of the test setup.

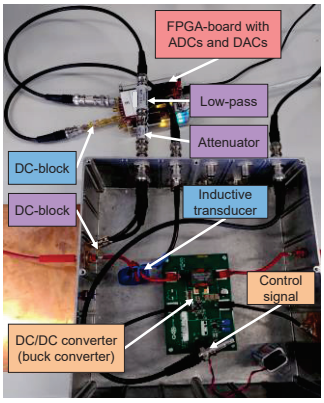

Fig. 5: Photograph of the inside of the DUT box.

5 Time-domain measurements during transient changes of the buck converter's operation

To evaluate the performance of the FPGA-based active EMI cancellation system during the buck converter's transient changes in operation, the resulting spectrogram of the residual noise will be determined. Hereby, the residual noise spectrum is visualized over time.

5.1 Spectrogram calculation for evaluation purposes

Because of the fast changes of the buck converter's operation modes, the determination of the (residual) noise signal's spectrogram is challenging. Due to the relatively slow measurement with help of common frequency-domain measurement equipment (e.g. EMI test receivers), the (residual) noise signal is initially measured in time domain with the help of an oscilloscope. Afterwards, the spectrogram of the residual noise signal is determined by the subsequent and successive calculation of the **F**ast **F**ourier **T**ransform (FFT) of several time segments of the measured residual noise signal as illustrated in Fig. 6. To do so, a time window of the measured residual noise signal is selected $(T_{\mathrm{Window}} = 10 / f_0)$, its FFT is calculated and assigned to the end time t_{End} of the regarded time window. Afterwards, the window is moved forward to calculate the next FFT. In the spectrogram all calculated FFTs are concatenated.

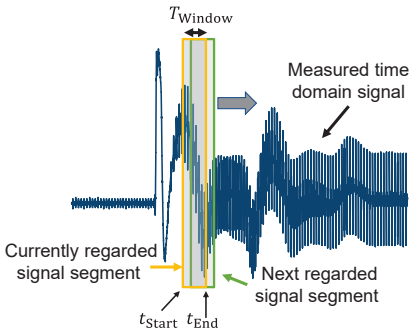

Fig. 6: Illustration of the spectrogram calculation.

5.2 Performance analysis during the switch-on of the adaptive notch filters

To examine the dynamic performance of the adaptive notch filter implementation, the noise suppression is initially analyzed during the switch-on process of the adaptive notch filter

implementation. To do so, the buck converter is operating in stationary mode and the (residual) noise signal is measured at the measurement port of the artificial network.

In Fig. 7, the corresponding spectrograms are depicted for two different step sizes ($\mu = 0.00067$ and $\mu = 0.002$). At $t = 0$, the six parallel adaptive notch filters are turned on and optimize the respective cancelling sine waves. The (residual) noise levels at the switching harmonics (harmonics of the switching frequency) decrease faster in case of the larger step size μ. This observation is especially noticeable for the switching frequency $f_0 = 300\,\mathrm{kHz}$ and its first two overtones at $600\,\mathrm{kHz}$ and $900\,\mathrm{kHz}$, due to their relatively high noise levels.

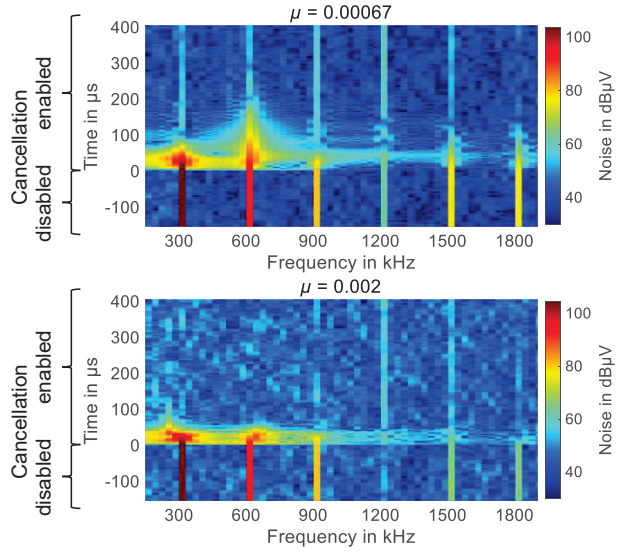

Fig. 7: Spectrograms of the (residual) noise during the switch-on process of the adaptive notch filters for two different step sizes.

5.3 Performance analysis during an exemplary change of the control signal's duty cycle

In the previous examination, the duty cycle of the buck converter's control signal has been constant. In the following, the performance of the adaptive notch filter implementation is examined during a changing duty cycle of the buck converter's control signal. The duty cycle is varied between 15 % and 25 % and comes along with a changing DC voltage at the ohmic load.

In the upper spectrogram in Fig. 8, the adaptive notch filter is turned off, while the duty cycle of the buck converter's control signal changes at $t = 0$. Obviously, the noise levels of the considered switching harmonics are stable for $t < 0$. After the duty cycle has changed, the noise levels stabilize again after a short period of time. The centrally placed and lower spectrogram in Fig. 8 reveal the behavior of the adaptive notch filter implementation for the two different step sizes during the variation of the duty cycle. Before the duty cycle changes ($t < 0$), the residual noise levels for both step sizes are below the measurement noise level. When the duty cycle changes at $t = 0$, the residual noise levels increase for every considered switching harmonic for both step sizes and temporarily exceed the corresponding noise levels with disabled notch filters. After the duty cycle changed and the noise signal stabilizes again, both adaptive notch filter implementations are able to quickly adapt to the changed noise signal. Here, the implementation with the larger step size parameter μ shows a faster adaptation of the anti-noise signal to the changed noise signal.

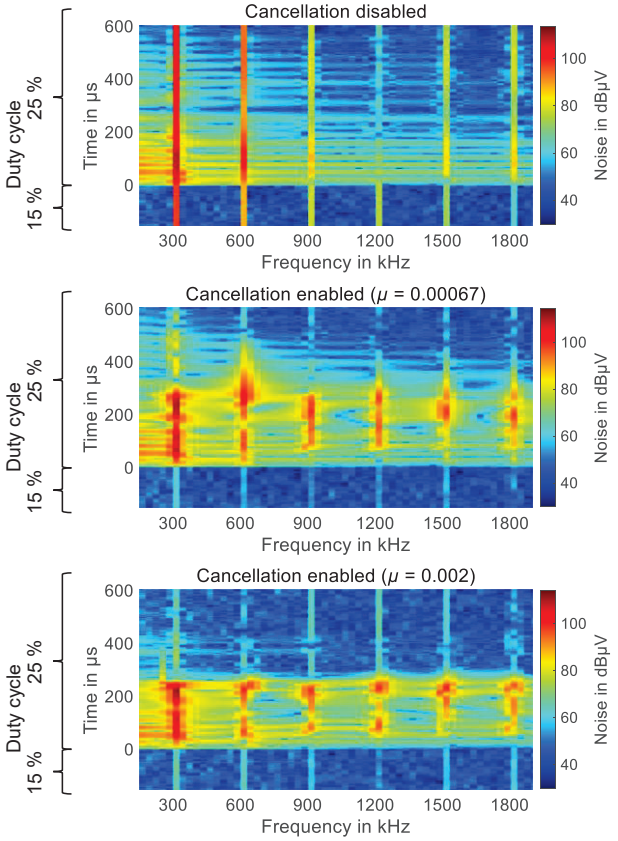

Fig. 8: Spectrograms of the (residual) noise in a time frame around the jump of the duty cycle of the buck converter's control signal.

Due to the suddenly changing duty cycle of the buck converter's control signal, the noise signal is changing, too. The previously found filter weights and the corresponding anti-noise signal do not fit

to the noise signal anymore. In consequence, a temporary amplification of the noise signal can occur (constructive interference). As soon as the noise signal stabilizes, both adaptive notch filter implementations quickly accomplish a significant noise reduction again (destructive interference).

5.4 Performance analysis during an exemplary change of the load resistance

In the previous examinations, the load resistance of the buck converter is kept constant at 1 Ω. Now, the load resistance at the 12 V-side of the buck converter initially equals 2 Ω, but, around $t = 0$, the load resistance is changed from 2 Ω to 1 Ω.

In case of the upper spectrogram in Fig. 9, the adaptive notch filter implementation is disabled, while noise levels at the considered switching harmonics are only slightly changing due to the changing load resistor. The spectrogram for the enabled notch filter implementation with the smaller step size of $\mu = 0.00067$ reveals stable noise reductions for all considered switching harmonics before, after and even during the changing of the load resistance. Similar results have been found for $\mu = 0.002$. In case of the changing load resistor, the disturbances seem to change more slowly compared to the case of the suddenly changing duty cycle from 15 % to 25 %. In consequence, the adaptation process can follow the changing noise signal, and the adaptive notch filters are able to achieve a sustained high noise suppression.

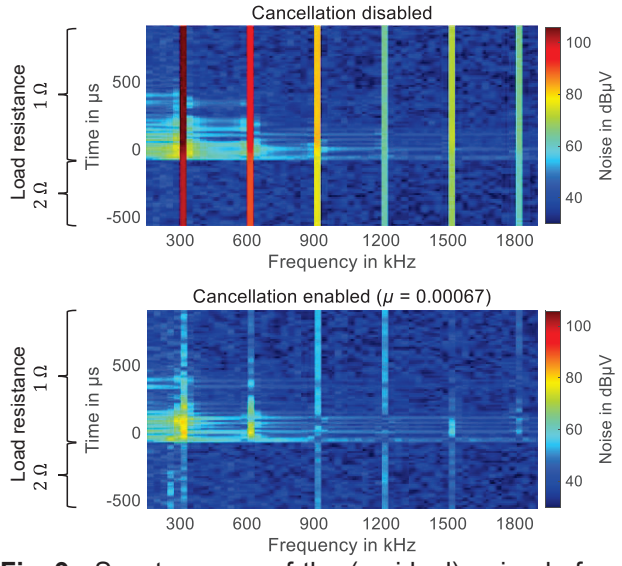

Fig. 9: Spectrograms of the (residual) noise before and after the load resistance change.

6 Frequency-domain measurements for transient changes of the buck converter's operation

The spectrograms in the previous sections are helpful to investigate the dynamic behavior of the adaptive notch filters. But finally, the method has to be evaluated with the help of EMI receiver measurements according to common EMC standards that are carried out and discussed below.

The previously shown analysis reveals that the examined adaptive notch filters may follow slowly changing noise signals. In contrast, sudden changes of the noise signal - e.g. caused by a suddenly changing duty cycle - can push the adaptive notch filter implementation to its limits.

The variation of the duty cycle of the buck converter's control signal can be realized in different ways and is therefore suitable for a further analysis of the notch filter's adaptation limits. In the following investigation, the duty cycle is varied either sinusoidal or rectangular between 15 % and 25 % as illustrated in Fig. 10. The sinusoidal variation of the duty cycle comes along with a more continuously changing noise signal, while the rectangular variation of the duty cycle causes sudden changes of the noise signal. By varying the modulation frequency $f_{\mathrm{Modulation}}$, the incidence of the larger and sudden duty cycle changes can be varied, while in case of the sinusoidal variation of the duty cycle, the speed of the duty cycle's alteration can be varied.

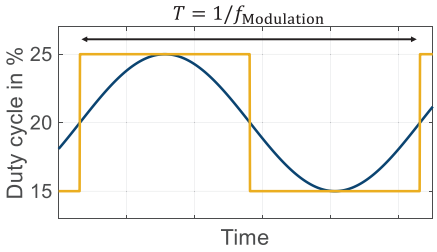

Fig. 10: Sinusoidal and rectangular variation of the buck converter's duty cycle.

In the following, the frequency of the sinusoidal or rectangular duty cycle modulation is varied between 100 mHz and 1 kHz. The buck converter is in operation and the adaptive notch filter is implemented with a step size $\mu = 0.002$. For evaluation purposes, the noise signal (disabled notch filters) and the residual noise voltages (enabled notch filters) are measured at the artificial network's measurement port by an EMI receiver

with 9 kHz resolution bandwidth and 20 seconds measurement time (so that at least two full cycles of the modulation are measured). The measurement is done with an average and a peak detector.

In Fig. 11, the realized noise reductions at the six considered switching harmonics are depicted for five different modulation frequencies $f_{\mathrm{Modulation}}$. The depicted noise reductions relate to either a sinusoidal (blue, yellow) or rectangular (violet, green) modulation of the duty cycle. The noise reductions in dB are calculated by subtracting the (residual) noise levels, measured at the observed switching harmonics.

In case of the rectangular modulation of the duty cycle, the peak-rated noise reductions are significantly lower than for the measurements with average-detector. Due to the sudden changes of the noise signal, the anti-noise signal does temporarily not fit to the noise signal anymore, as described in detail in Section 5.3. In consequence, the noise signal can be momentarily amplified (constructive interference), such that the residual noise level exceeds the noise level. This momentary amplification is captured by the peak detector measurement of the residual noise signal. In consequence, the determined noise reduction in peak-mode is vanishingly small (300 kHz, 600 kHz), or even negative (900 kHz – 1.8 MHz). The peak detector finds the highest value during the measurement time without considering the repetition rate of the disturbance. So, the peak-rated values are independent from the modulation frequency. After the abrupt changes, the adaptive notch filters have quickly adapted the anti-noise signal and a significant noise reduction is achieved most of the time. Consequently, a significant noise reduction is determined by measuring the average-rated (residual) noise signals. The higher the modulation frequency is chosen, the more often the duty cycle changes and the more often a temporary amplification of the noise signal occurs. In consequence, the noise reduction in average-mode decreases with higher modulation frequency.

In case of a sinusoidal modulation of the control signal's duty cycle, the noise reductions determined by measurements with average and peak detector are very similar. This indicates that the adaptive notch filters can follow the changes of the noise signal due to the continuously changing duty cycle of the control signal. The depicted noise reductions for all considered switching harmonics reveal that the achieved noise reductions are decreasing with increasing modulation frequency above a modulation frequency of 10 Hz. Nonetheless, even at the higher switching harmonics and the highest regarded modulation frequency (1 kHz), the achieved noise reduction is nearly 20 dB for the average- and peak- rated emissions.

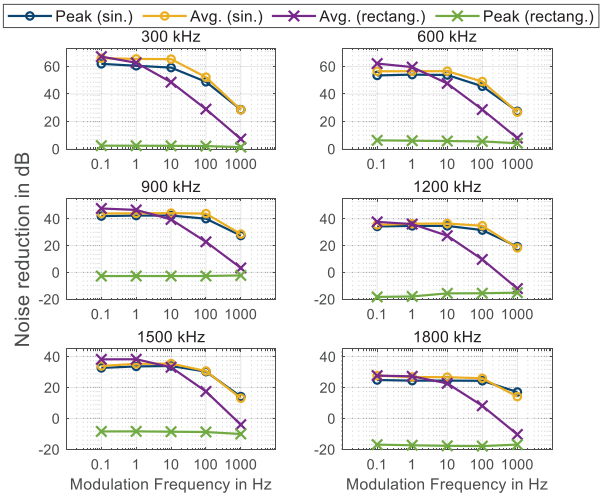

Fig. 11: Noise reductions at the switching harmonics for different modulation frequencies.

7 Conclusion and Outlook

In this work, an FPGA-based adaptive notch filter has been examined during different transient changes of a buck converter's operation mode, e.g. a suddenly changing duty cycle of the control signal, or a changing load resistance.

Suddenly changing noise signals, e.g. caused by a suddenly changing duty cycle of the control signal, can push the adaptive notch filter to its limits and may cause a temporary amplification of the noise signal. This suddenly changing noise signal does not fit to the previously found anti-noise signal anymore and the adaptation process needs some time to fit the anti-noise signal to the changed noise signal again.

In contrast, a slowly or more continuously changing noise signal allows the adaptive notch filters to follow the noise signal's changes. In case of a sinusoidal modulation of the duty cycle of the buck converter's control signal, noise reductions of e.g. 65 dB (average detector) and 59 dB (peak detector) have been realized at 300 kHz with a modulation frequency of 10 Hz. The realized noise reductions slowly decrease for modulation frequencies above 10 Hz, but still reveal the potential of the method with a noise reduction of e.g. around 50 dB at 300 kHz and 24 dB at 1.8 MHz with a modulation frequency of 100 Hz.

The adaptive notch filter's ability to follow changing noise signals caused by a sinusoidal modulation of the control signal's duty cycle suggests the application to inverter systems and will be subject of future investigations.

8 References

[1] "CISPR 25 – Vehicles, boats and internal combustion engines – Radio disturbance characteristics – Limits and methods of measurement for the protection of on-board receivers," 4th ed., Feb. 2015.

[2] K. Mainali, R. Oruganti, "Conducted EMI mitigation techniques for switch-mode power converters: A Survey," IEEE Trans. Power Electron., vol. 25, no. 9, pp. 2344-2356, Sep. 2010.

[3] Y.-C. Son, S.-K. Sul: "Generalization of active filters for EMI reduction and harmonics compensation," IEEE Trans. Ind. Appl., vol. 42, no. 2, pp. 545-551, Mar.-Apr. 2006.

[4] N. K. Poon, J. C. P. Liu, C. K. Tse, M. H. Pong: "Techniques for input ripple current cancellation: classification and implementation [in SMPS]," IEEE Trans. Power Electron., vol. 15, no. 6, pp. 1144-1152, Nov. 2000.

[5] B. Narayanasamy, F. Luo, "A survey of active EMI filters for conducted EMI noise reduction in power electronic converters," IEEE Trans. Electromagn. Compat., vol. 61, no. 6, pp. 2040-2049, Dec. 2019.

[6] A. Bendicks, "Active cancellation of electromagnetic emissions of power electronic systems by injecting synthesized and synchronized signals," Ph.D. dissertation, On-board Systems Lab, TU Dortmund University, Dortmund, Germany, 2020. [Online]. Available: https://eldorado.tu-dortmund.de/handle/2003/39212?locale=en.

[7] A. Bendicks, M. Rübartsch, S. Frei, "Simultaneous EMI suppression of the input and output terminals of a DC/DC converter by injecting multiple synthesized cancellation signals," in Proc. Int. Symp. Electromagn. Compat. Eur., Barcelona, Spain, 2 - 6 Sep. 2019, pp. 842-847.

[8] S. M. Kuo, D. R. Morgan, "Active noise control: A tutorial review," Proc. IEEE, vol. 87, no. 6, pp. 943–973, Jun. 1999.

[9] S. M. Kuo, D. R. Morgan, "Active noise control systems – Algorithms and DSP implementations," New York: Wiley, 1996.

[10] A. Bendicks, T. Dörlemann, S. Frei, N. Hees, M. Wiegand, "FPGA-basierte aktive Gegenkopplung der Schaltharmonischen von leistungselektronischen Systemen," in Proc. Conf. Electromagn. Compat., Düsseldorf, Germany, 20 - 22 Feb. 2018, pp. 652-661.

[11] A. Bendicks, T. Dörlemann, S. Frei, N. Hees, M. Wiegand, "Development of an adaptive EMI cancellation strategy for stationary clocked systems," in Proc. Int. Symp. Electromagn. Compat. Eur., Amsterdam, Netherlands, 27-30 Aug. 2018, pp. 78-83.

[12] A. Bendicks, T. Dörlemann, S. Frei, N. Hees, M. Wiegand, "Active EMI reduction of stationary clocked systems by adapted harmonics cancellation," IEEE Trans. Electromagn. Compat., vol. 61, no. 4, pp.998-1006, Aug. 2019.

[13] A. Bendicks, A. Peters, S. Frei, M. Wiegand, N. Hees, "FPGA-basierte aktive Unterdrückung der elektromagnetischen Störungen einer aktiven Leistungsfaktorkorrektur (PFC) durch die Injektion von modulierten Sinussignalen," in Proc. Conf. Electromagn. Compat., Cologne, Germany, pp. 433-442, 12-13 May 2020.

[14] A. Bendicks, A. Peters, S. Frei, "FPGA-based Active Cancellation of the EMI of a Boost Power Factor Correction (PFC) by Injecting Modulated Sine Waves," IEEE Letters on Electromagnetic Compatibility Practice and Applications, vol. 3, no. 1, pp.11-14, March 2021.

[15] J. R. Glover, Jr., "Adaptive noise canceling applied to sinusoidal interferences," in IEEE Trans. Acoust., Speech, Signal Process., vol. 25, no. 6, pp. 484-491, Dec. 1977.

[16] E. Ziegler, Jr., "Selective active cancellation system for repetitive phenomena," U.S. Patent 4 878 188, 31 Oct. 1989.

[17] C. C. Boucher, S. J. Elliott, P. A. Nelson, "Effect of errors in the plant model on the performance of algorithms for adaptive feedforward control," IEE PROC-F., vol. 138, no. 4, pp. 313-319, Aug. 1991.